# Damping of Inter-Area Oscillations via Modulation of Aggregated Loads

Felipe Wilches-Bernal, *Member, IEEE*, Raymond H. Byrne, *Fellow, IEEE*, and Jianming Lian, *Member, IEEE*

***Abstract*—Low frequency electromechanical oscillations can pose a threat to the stability of power systems if not properly addressed. This paper proposes a novel methodology to damp these inter-area oscillations using loads, the demand side of the system. In the proposed methodology, loads are assigned to an aggregated cluster whose demand is modulated for oscillation damping. The load cluster control action is obtained from an optimal output feedback control (OOFC) strategy. The paper presents an extension to the regular OOFC formulation by imposing a constraint on the sum of the rows in the optimal gain matrix. This constraint is useful when the feedback signals are generator speeds. In this case, the sum of the rows of the optimal gain matrix is the droop gain of each load actuator. Time-domain simulations of a large-scale power system are used to demonstrate the efficacy of the proposed control algorithm. Two different cases are considered: a power imbalance and a line fault. The simulation results show that the proposed controllers successfully damp inter-area oscillations under different operating conditions and with different clustering for the events considered. In addition, the simulations illustrate the benefit of the proposed extension to the OOFC that enable load to provide a combination of droop control and small signal stability augmentation.**

***Index Terms*—Small signal stability, damping control, load modulation, load aggregation, system identification.**

## I. Introduction

SPARSELY interconnected power systems typically experience oscillations or power swings between disperse geographical areas. Synchronous generators in one geographic area oscillate against those in other areas. These oscillations are typically the result of weak connections or high power transfers between the areas [1]. Inter-area oscillations can threaten the stability of the system if not properly controlled. The 1996 West Coast Blackout in the United States was partially attributed to poorly damped inter-area oscillations [2].

One solution to address inter-area oscillations is to limit the amount of power transfer in critical tie lines in order to reduce the stress in the system. Although effective, this solution is far from optimal as it results in underutilization of transmission line infrastructure [3]. Another commonly considered solution is to implement power system stabilizers (PSSs) in conventional generators dispersed throughout the system [4]. PSSs add damping to inter-area oscillations by modulating the input signal to the generator excitation system. To improve damping PSSs must be in the correct location. Traditionally, PSSs are enabled with local signals but the use of remote signals has been proven useful in enhancing their damping action [5]. The use of remote measurements for damping inter-area oscillations, referred to as wide-area damping control, has been extensively studied [6]–[9]. Previous research has identified a number of potential actuators for improving damping in electric power systems. This includes: FACTS devices [10]–[12], energy storage [13], [14], wind power plants [15]–[18], solar PV plants [19], [20] and high-voltage direct current (HVDC) links [21], [22]. HVDC links have also been demonstrated to work in practice. A controller for inter-area oscillation damping has been implemented by modulating the power transfer of the Pacific DC Intertie, the longest HVDC line in the United States [21], [23]. This controller uses wide-area measurements from phasor measurement units (PMUs) installed within the western North American Power System (wNAPS).

The idea of using end-use loads on the demand side to damp inter-area oscillations has been proposed previously [24]–[26]. In [24], [25] a novel device-level control strategy was proposed to deliver the aggregator-level load modulation signal. However, the aggregator-level load modulation signal used in [24], [25] is identical to that in [21] which is determined by a proportional control based on the feedback of frequency difference (note that the work in [21] uses an HVDC link as the actuator).

In this paper, a novel methodology is proposed to determine the aggregator-level load modulation signal. The methodology starts by grouping the loads into clusters where they are controlled as a unit. The system is then probed to obtain generator speeds as outputs which are consequently aggregated into areas. Using the probing signal as an input and the area generator speeds as outputs, the methodology uses the Eigenvalue Realization Algorithm (ERA) to estimate a linear representation of the system [27]. Assuming the only information available for control is the aggregated generator speeds, the next step of the methodology is to design a controller. Optimal output feedback control (OOFC) theory is employed for this task. The paper proposes a modification to this technique to ensure that the rows of the optimal gain matrix add up to a prescribed value. This is because the sum of the values of a particular row of the control gain matrix is the droop (or steady-state gain) of

Manuscript received February 24, 2019; revised June 26, 2019; accepted October 12, 2019. Date of publication October 18, 2019; date of current version April 22, 2020. This work was supported by the Grid Modernization Lab Consortium (GMLC) program funded by U.S. DOE. Paper no. TPWRS-00282-2019. *(Corresponding author: Felipe Wilches-Bernal.)*

F. Wilches-Bernal and R. H. Byrne are with Sandia National Laboratories, Albuquerque, NM 87185 USA (e-mail: fwilche@sandia.gov; rhbyrne@sandia.gov).

J. Lian is with Pacific Northwest National Laboratory, Richland, WA 99352 USA (e-mail: jianming.lian@gmail.com).

Color versions of one or more of the figures in this article are available online at http://ieeexplore.ieee.org.

Digital Object Identifier 10.1109/TPWRS.2019.2948116

the corresponding load actuator. To illustrate the effectiveness of the proposed methodology the paper includes time-domain simulations of a large-scale power system representative of the wNAPS. The paper also studies the impact that the operating condition of the power system has on the performance of the proposed control strategies. In addition, the paper analyses the effect that load clustering has on the effectiveness of the control action. The paper details how aggregator-level load modulation can be realized with detailed end-use load models.

The remainder of this paper is organized as follows. Section II details the methodology to cluster loads, aggregate generators, and perform system identification. Section III presents the approach to include constraints to the optimal output feedback control. Section IV introduces the test system and presents the stabilizing controllers. Section V presents simulations in time domain that show the effectiveness of the proposed controllers in providing damping to the system. Section VI analyzes the effect of the operating condition and system topology on the efficacy of the controllers. Section VII presents the impact of load clustering on the performance of the controllers. Section VIII shows how the load action demanded by the controllers can be achieved with detailed end-use load models. Finally, Section IX presents concluding remarks of the paper as well as future avenues of research.

## II. System Clustering and Identification

Power systems are composed of multiple load and generation centers. For a large power system, each load or generation station does not constitute more than a small percentage of the total power consumed or produced, respectively. As such, moderate movements at each individual load or generation unit have little effect on the total dynamics of the system. The methodology proposed in this paper clusters loads so that each load cluster is modeled as a single actuator. Loads can be clustered by geographical or electrical distances or because their signals are highly correlated with each other. Based on analysis of the western North American power system, mode shape tends to stay relatively constant over long periods (e.g., at least several years for the WECC) [28]. Mode frequency and mode damping change with the system operating conditions. Therefore, a clustering design would have to be updated relatively infrequently for a typical power system.

In this work, machine speeds are used as the feedback measurement signals for control design. Note that machine speeds are exactly the type of signals where inter-area oscillations are observable. This is because inter-area oscillations are power swings between different geographical areas that directly impact rotational speeds of generators within those areas. Because there can be multiple generators in an individual area, the methodology proposed in this paper relies on a weighted average machine speed for each area given by

$$\omega_a = \frac{1}{H_a} \sum_{i \in \Omega_a} H_i \omega_i \tag{1}$$

where $\omega_a$ is the *area* $a$ speed (or frequency) to be used as a feedback signal, $\Omega_a$ is the set of generators in area $a$, $H_i$ is the inertia constant of the $i$th generator, and

$$H_a = \sum_{i \in \Omega_a} H_i \tag{2}$$

is the total inertia in $\Omega_a$. Fig. 1 shows an example of the clustering of loads and aggregation of generator speeds employed in this paper. It is important to note that averaging generator speeds and bus frequencies has shown benefits for synthetic inertia and droop control [29], [30]. An example of the area speed by averaging generator speeds in a test power system is presented in Section IV. Note the details of load and generator clustering are beyond the scope of this paper.

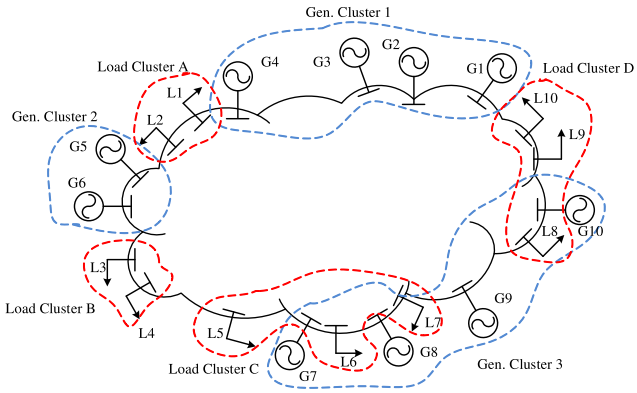


Fig. 1. Generator and load clustering example.

### A. System Identification

In order to determine the effect load clusters have on the dynamics of the system, system identification is performed by stimulating the system model with a set of probing signals. These tests consist of modulating the active power of every load cluster simultaneously with the same test signal. That is, the power modulation command for a particular load $i$ in a given cluster $\mathcal{C}$ is

$$P_{i,\mathrm{cmd}}(t) = \alpha P_{i,\mathrm{schd}} x_{\mathrm{prb}}(t) \qquad \forall i \in \mathcal{C} \tag{3}$$

where $P_{i,\mathrm{schd}}$ is the scheduled or steady-state power consumption at the $i$th load, $\alpha$ is an amplitude multiplier, and $x_{\mathrm{prb}}(t)$ is any probing signal. Note that the form of (3) ensures that the modulation of every load is the same in percentage terms. In this work, the selected probing signal is an exponential chirp which is described by

$$x_{\mathrm{prb}}(t) = \sin\left(\frac{2\pi f_s (r_f^t - 1)}{\ln(r_f)}\right) \tag{4}$$

with

$$r_f = \left(\frac{f_e}{f_s}\right)^{1/T} \tag{5}$$

where $f_s$ and $f_e$ are the starting and ending frequencies of the chirp signal and $T$ is the duration of it. An example of the probing is presented in Fig. 5 in Section IV which further explains it in the context of an example.

**Algorithm 1:** System Identification Algorithm.

**for** $i = 1 : m$ **do**
  Stimulate $i$th load with a logchirp signal, $u_i(t)$
  Calculate the Fourier Transform of the logchirp signal, $U_i(w) = \mathscr{F}(u_i(t))$
**end for**
**for** $j = 1 : p$ **do**
  Filter the $j$th area speed response (if necessary) via zero-phase digital filtering
  Calculate the Fourier Transform of the $j$th area speed response $\Omega_{aj}(w) = \mathscr{F}(\omega_{aj}(t))$
  Filter the Fourier Transform of the $j$th area speed response (if necessary), $\Omega_{aj}(w)$
**end for**
**for** $i = 1 : m$ **do**
  **for** $j = 1 : p$ **do**
    Calculate the impulse response from the $i$th input to the $j$th output, $y_{ij}(t) = \mathscr{F}^{-1}(\Omega_{aj}(w)/U_i(w))$
    Filter the impulse response $y_{ij}(t)$ (if necessary) via zero-phase digital filtering
  **end for**
**end for**
Apply the MIMO ERA algorithm, using the ratio of singular values to identify the appropriate order of the model, to estimate the state space system model

The purpose of the probing is to capture the behavior of each of the *area frequencies* in (1). Having the probing signal as an input and the multiple area frequencies as outputs, system identification techniques can be used to estimate the state space model of the system. Note that because the probing is performed independently for each area, the identification is initially performed as a SIMO system. Then by combining the results for all the independent probing test the identification of the MIMO system is accomplished. The system identification technique used in this work is based on the well known ERA [27]. The system identification algorithm is described in more detail in Algorithm 1. The output of this technique is a state space representation of the system in the following form

$$\dot{x}(t) = Ax(t) + Bu(t) \tag{6}$$

$$y(t) = Cx(t) \tag{7}$$

where $x \in \mathbb{R}^n$ is the state, $u \in \mathbb{R}^m$ is the control input, $y \in \mathbb{R}^p$ is the output. In this case, $m$ is the number of load clusters and $p$ correspond to the number of generator areas. The goal of the proposed methodology is to identify a linear model that captures the input-output dynamics of the load clusters and the generator area speeds. There are many potential system identification techniques that may be employed to estimate the state space model of the power system [31]. ERA was selected because of the prior demonstrated successful application to electric power systems [32].

## III. Optimal Output Feedback Control Design

The control approach proposed in this paper, depicted in Fig. 2, aims at computing the optimal gain $K$ to modulate the clusters of loads ($\Delta P_{cl,k},\ \forall k = 1 \dots m$) having only the information of the output measurements which are the *area frequencies*. This is the typical optimal output feedback problem where the control law is restricted to use only information from the outputs $y$. For the system in (6) this is expressed as

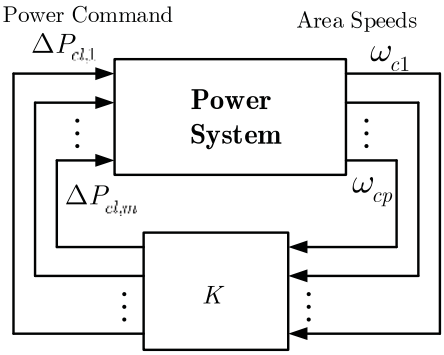


Fig. 2. Control approach proposed.

$$u(t) = Ky(t) \tag{8}$$

where $K \in \mathbb{R}^{m \times p}$. Note that

$$u = [\Delta P_{cl,1} \ \dots \ \Delta P_{cl,m}]^\top, \qquad y = [\omega_{a1} \ \dots \ \omega_{ap}]^\top \tag{9}$$

The optimal output feedback control problem can be formulated as follows. The performance index (or cost function) to minimize is [33]

$$\tilde{J} = \mathbb{E}\left\{ \int_0^\tau x(t)^\top \left(Q + C^\top K^\top RKC\right) x(t) dt + x(\tau)^\top S_f x(\tau) \right\} \tag{10}$$

where $\mathbb{E}\{\cdot\}$ denotes the expected value and

$$\mathbb{E}\left\{x_0 x_0^\top\right\} \triangleq X_0 \tag{11}$$

is the covariance of the initial conditions. The optimization is then formulated as

$$\min_K \ \tilde{J}(K, \tau) \tag{12}$$

where $K$ is assumed to exist and is to be chosen from the set $\mathcal{S}$ of stabilizing gains defined as

$$\mathcal{S} \triangleq \{K \in \mathbb{R}^{m \times p} : \text{Re}\{\lambda(A + BKC)\} < 0\} \tag{13}$$

The OOFC problem has been solved before using different approaches [33]–[36]. A straightforward method consists of using the general results obtained for scalar-valued composite functions of matrices [34], [36]. In this approach, having

$$X = x(t)x(t)^\top \tag{14}$$

the problem is then rewritten as [34]

$$\min_K \ \tilde{J}(K, \tau) = \int_0^\tau \text{tr}\left\{(Q + C^\top K^\top RKC)X\right\} \ dt + \text{tr}\left\{x^\top S_f x\right\} \tag{15}$$

subject to

$$\dot{X}(t) = (A + BKC)X(t) + X(t)(A + BKC)^\top \tag{16}$$

The problem in (15) is solved by using the Hamiltonian function as follows

$$H(X, \Lambda, K) = \text{tr}\{(Q + C^\top K^\top RKC)X\} + \text{tr}\{\Lambda^\top[(A + BKC)X + X^\top(A + BKC)]\} \tag{17}$$

where $\Lambda$ is the Lagrange multiplier used to include the condition in (16) into the problem. According to the lemma and corollary in Section II-2 in [34], the gradient matrix with respect to $K$ of $\tilde{J}(K, \tau)$ in (15) is

$$\frac{\partial \tilde{J}}{\partial K} = 2\left(RKC + B^\top \Lambda\right) \int_0^\tau X \, dt \, C^\top \tag{18}$$

with the stationarity conditions

$$\frac{\partial H}{\partial X} = -\dot{\Lambda} = Q + C^\top K^\top RKC + \Lambda(A + BKC) + (A + BKC)^\top \Lambda \tag{19}$$

$$\frac{\partial H}{\partial \Lambda} = \dot{X} = (A + BKC)X + X(A + BKC)^\top \tag{20}$$

$$\Lambda(\tau) = S_f \qquad X(0) = X_0 \tag{21}$$

When considering the infinite horizon case (i.e. when $\tau \to \infty$), with $S_f = 0$, the necessary conditions for optimality can be written as [34]

$$0 = Q + C^\top K^\top RK + \Lambda(A + BKC) + (A+BKC)^\top \Lambda \tag{22}$$

$$0 = (A + BKC)P + P(A + BKC)^\top + X_0 \tag{23}$$

$$0 = \frac{\partial \tilde{J}}{\partial K} = 2\left(RKC + B^\top \Lambda\right) PC^\top \tag{24}$$

where $P$ is

$$\int_0^\infty X \, dt = P \tag{25}$$

Then the optimal gain $K^*$ can be obtained from (24) as

$$K^* = -R^{-1}B^\top \Lambda P C^\top (CPC^\top)^{-1} \tag{26}$$

Note that relationships (22)–(23) are Lypunov-type equations and together with equation (24) form a system of coupled matrix equations. Such a system can be numerically solved by different computational methods such as the Anderson-Moore and Quasi-Newton [37].

In order to achieve the dual control goals of improved damping and frequency droop control, an additional constrain is proposed on the optimal gain $K$, which is the solution of the optimal output feedback control problem. Considering the optimal gain can be written as

$$K = \begin{bmatrix} k_{11} & k_{12} & \dots & k_{1p} \\ k_{21} & k_{22} & \dots & k_{2p} \\ \vdots & \vdots & \ddots & \vdots \\ k_{m1} & k_{m2} & \dots & k_{mp} \end{bmatrix} \tag{27}$$

The optimal modulation command of the $i$th cluster of loads is expressed by

$$\Delta P_{cl,i} = \sum_{j=1}^{p} k_{ij}\omega_{aj} \qquad \forall i = 1 \dots m \tag{28}$$

Note that in the type of problem this paper addresses, the feedback signals are frequencies (more accurately average area frequencies) whose steady state operating condition converges to the same value $\omega_F$ (provided that the system remains in synchronism). That is,

$$\omega_{aj}(t) = \omega_F \qquad \forall j = 1 \dots p \tag{29}$$

when $t \to \infty$. This feature is important because it means that the sum of the rows of $K$ represent the droop gain for a particular load cluster. Following the development in [38] for OOFC a method to fix the sum of the rows of gain $K$ to particular values is presented. The proposed method modifies the performance index in (10) with a penalty function to include the constraint. To impose this structure, consider a matrix $T_j \in \mathbb{R}^{p\times n}$ with all its elements equal to zero except those in its $j$th column which have a value of 1. The penalty function to ensure the sum of the rows is equal to $\bar{v}$ is defined as

$$g(K) = \gamma T_j^\top (K - \Upsilon)^\top (K - \Upsilon) T_j \tag{30}$$

where $\Upsilon \in \mathbb{R}^{m\times p}$ is

$$\Upsilon = \bar{v}\frac{\mathbf{1}_p^\top}{p}. \tag{31}$$

Note that any of the $p$ columns of $T_j$ can be the one with the values at 1, and for this reason the subindex $j$ will be dropped from $T_j$ henceforth. Note also that $\gamma$ is a scalar used as a parameter to adjust the penalty on the sum of the rows of $K$. The weight $\gamma$ can be adjusted depending on the importance of strictly adhering to the constraint. Including the penalty function $g$, the cost function to minimize becomes

$$\tilde{J}(K, \tau) = \mathbb{E}\left\{\int_0^\tau x(t)^\top \Big(Q + C^\top K^\top RKC + \gamma g(K)\Big) x(t) \, dt + x(\tau)^\top S_f x(\tau)\right\} \tag{32}$$

Then the optimization problem to be solved is

$$\min_K \ \tilde{J}(K, \tau) \tag{33}$$

subject to (16) and where $K$ is again to be chosen from the set $\mathcal{S}$ defined in (13). Following the approach in [34], the Hamiltonian

function for this case becomes

$$H = \text{tr}\Big\{\Big(Q + C^\top K^\top RKC + \gamma T^\top (K-\Upsilon)^\top (K-\Upsilon)T\Big\} + \text{tr}\Big\{\Lambda^\top\Big((A+BKC)X + X^\top (A+BKC)\Big)\Big\} \quad (34)$$

and the gradient matrix with respect to $K$ of $\tilde{J}(K,\tau)$ in (33) is

$$\frac{\partial \tilde{J}}{\partial K} = 2\left(RKC + B^\top \Lambda\right)\int_0^\tau X dt\, C^\top + 2\gamma KT\int_0^\tau X dt\, T^\top - 2\gamma \Upsilon T\int_0^\tau X dt\, T^\top \quad (35)$$

where the stationarity conditions are

$$\frac{\partial H}{\partial X} = -\dot{\Lambda} = Q + C^\top K^\top RKC + \gamma T^\top (K-\Upsilon)^\top (K-\Upsilon)T + \Lambda(A+BK) + (A+BK)^\top \Lambda \quad (36)(37)$$

$$\frac{\partial H}{\partial \Lambda} = \dot{X} = (A+BKC)X + X(A+BKC)^\top \quad (38)$$

$$\Lambda(\tau) = S_f \qquad X(0) = X_0 \quad (39)$$

When $\tau \to \infty$, the infinite horizon case, and with $S_f = 0$, the necessary conditions for optimality become

$$0 = Q + C^\top K^\top RK + +\gamma T^\top (K-\Upsilon)^\top (K-\Upsilon) + \Lambda(A+BKC) + (A+BKC)^\top \Lambda \quad (40)$$

$$0 = (A+BKC)P + P(A+BKC)^\top + X_0 \quad (41)$$

$$0 = \frac{\partial \tilde{J}}{\partial K} = 2\left(RKC + B^\top \Lambda\right)PC^\top + 2\gamma KTPT^\top - 2\gamma \Upsilon TPT^\top \quad (42)$$

This last relationship can be reorganized as,

$$B^\top \Lambda PC^\top - \gamma \Upsilon TPT^\top + RKCPC^\top + \gamma KTPT^\top = 0 \quad (43)$$

Note that this final equation is a Sylvester equation in $K$. Relationships (40) and (41) are Lyapunov equations, and (42) is a Sylvester equation. Solving this system of equations yields a solution to problem (33).

## IV. Test Power System and Control Design

In order to demonstrate the efficacy of the proposed control design, simulation results are presented for a reduced-order representation of the wNAPS, known as the MinniWECC. This topology of the system is shown in Fig. 3 [39]. The load and generation clustering as well as the control strategy proposed in Section II were evaluated on this representative system. The model has 34 generators, 120 buses, 19 loads and two HVDC transmission lines. This model has all the small signal dynamics of the actual wNAPS. The operating condition of the system was adjusted so that the North South B (or Alberta) mode exhibits low damping.

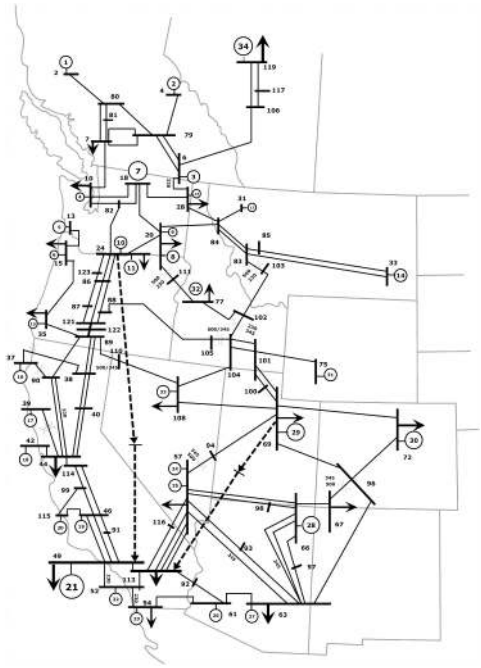

Fig. 3. The miniWECC, a reduced order representation of the western interconnection.

TABLE I
Load Clusters in the MiniWECC

| Cluster No. | Loads in the cluster | Total power (MW) |
|---|---|---|
| 1 | $L_{21}$, $L_{26}$, $L_{16}$, $L_{36}$ | 5850 |
| 2 | $L_{29}$, $L_{11}$, $L_8$ | 11375 |
| 3 | $L_{55}$, $L_{56}$, $L_{64}$, $L_{95}$, $L_{73}$, $L_{120}$ | 41375 |
| 4 | $L_{78}$, $L_{43}$, $L_{109}$ | 17340 |
| 5 | $L_{112}$, $L_{50}$, $L_{70}$ | 30075 |

In this work, the loads of the miniWECC are divided in the five clusters listed in Table I. Each of these clusters is controlled as a unit, as explained in Section II. The clusters were identified using a correlation algorithm on measurement data. Fig. 4 shows the individual bus frequencies for two of the load clusters for a disturbance event in the system. This figure show that individual frequencies within a cluster are very similar to each other. Note that even though in this example every one of the 19 loads in the system were assigned to a cluster, this is not necessary in the proposed method. That is there are loads that are exempt of being modulated, similarly there can be clusters of size one (e.g., a case of a large load).

The generators present in the system are grouped into 6 areas as presented in Table II. The selection of the areas was performed in a similar fashion as the load clustering due to high correlation in machine speed signals. In this case, Generator 26 at Bus 61 is not included in any area.

A linearized system model was obtained using the system identification approach described in Section II-A. The probing signal is an exponential chirp, for approximately 60 seconds, with a starting frequency of $f_s = 0.1$ Hz and an ending frequency of $f_e = 3$ Hz. Note that the actual duration of the probing is adjusted such that the initial and ending points of the chirp

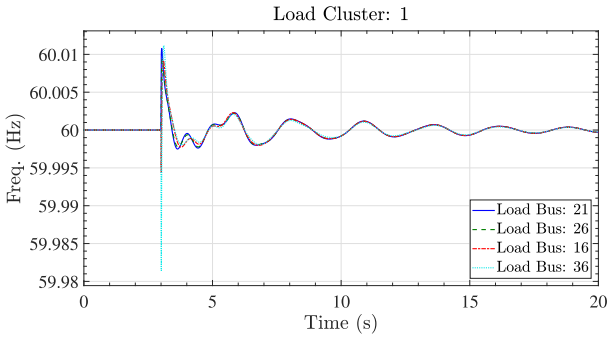


**(a)** Cluster No. 1.

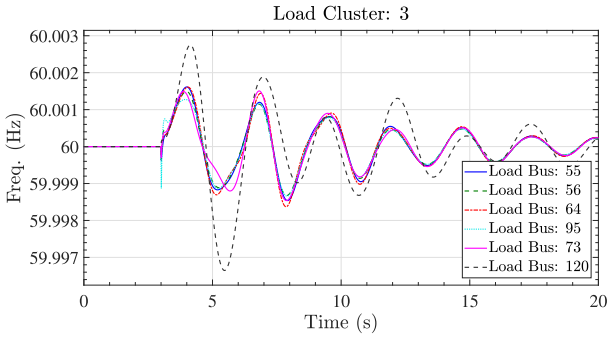


**(b)** Cluster No. 3.

Fig. 4. Bus frequencies at different load buses, (a) load buses of Cluster No.1 and (b) load buses of Cluster No 3.

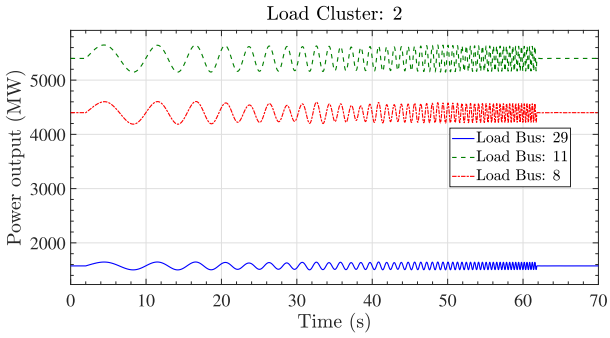


Fig. 5. Power output of loads in a particular cluster when probing using a chirp signal.

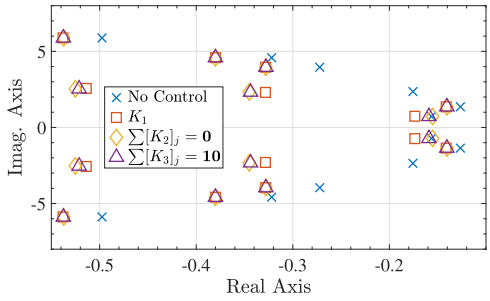


Fig. 6. Poles of the identified system in open and closed loop.

TABLE II
GENERATORS AREAS

| Area No. | Generators in Area |
|---|---|
| 1 | $G_8$, $G_9$, $G_{10}$, $G_{11}$, $G_5$, $G_{15}$ |
| 2 | $G_5$, $G_{13}$, $G_{14}$, $G_{12}$, $G_7$ |
| 3 | $G_{22}$, $G_{30}$, $G_{25}$, $G_{24}$, $G_{28}$, $G_{27}$, $G_{23}$, $G_{34}$ |
| 4 | $G_{19}$, $G_{20}$, $G_{21}$, $G_{29}$ |
| 5 | $G_{16}$, $G_{17}$, $G_{18}$, $G_{31}$, $G_{32}$, $G_{33}$ |
| 6 | $G_1$, $G_2$, $G_3$, $G_4$ |

signal are zero. Starting and ending the chirp signal at a zero value avoids sharp discontinuities which unnecessarily excites frequencies beyond the range of interest. Fig. 4 shows the power levels of the loads in Cluster 2 when this cluster is being used to perform the probing. The identified system has 44 states, 5 inputs and 6 outputs, that is, $x \in \mathbb{R}^{44}$, $u \in \mathbb{R}^5$, and $y \in \mathbb{R}^6$. The poles of the identified system are shown in Fig. 6 with the blue crossed markers.

Using the identified system, three different stabilizing controllers were designed with the strategy outlined in Section III:

- The first controller, noted $K_1$, is presented in (44) and is product of the regular optimal output feedback control.
- The second controller has the gain shown in (45) and is the result of imposing a constraint on the rows of the optimal gain. In this particular case the value selected was zero for all the rows of the gain (i.e. $\sum[K]_j = \mathbf{0}$). This restriction is achieved with the proposed control strategy detailed in Section III.
- The third controller results in the gain in (46) and is the case where the sum of each row of the optimal gain is equal to 10 (i.e. $\sum[K]_j = \mathbf{10}$).

Note that the sum of the rows of $K_1$ is $[13.54\ 30.93\ 61.58\ 32.88\ 52.19]^\top$ which are all greater than ten. The poles of the system using these control gains are presented in Fig. 6 with the square and diamond markers, respectively. This result show that the controllers provide damping to the inter-area oscillations in the system.

$$K_1 = \begin{bmatrix} 10.52 & 18.88 & -6.27 & -0.92 & 1.67 & -10.34 \\ 25.14 & -7.49 & -6.21 & -4.58 & -6.64 & 30.72 \\ -10.81 & -17.63 & 115.69 & -38.82 & 2.08 & 11.06 \\ 2.77 & 19.94 & -19.29 & 14.12 & 37.14 & -21.80 \\ -21.56 & 26.86 & 0.70 & 70.16 & 5.07 & -29.05 \end{bmatrix} \quad (44)$$

$$K_2 = \begin{bmatrix} 9.18 & 17.20 & -11.39 & -3.17 & -0.018 & -11.80 \\ 22.38 & -11.68 & -17.94 & -9.72 & -10.52 & 27.47 \\ -17.47 & -24.14 & 91.73 & -48.90 & -5.67 & 4.44 \\ -0.51 & 15.85 & -31.69 & 8.75 & 32.96 & -25.36 \\ -26.82 & 20.68 & -19.34 & 61.67 & -1.46 & -34.72 \end{bmatrix} \quad (45)$$

$$K_3 = \begin{bmatrix} 10.25 & 18.36 & -7.61 & -1.54 & 1.22 & -10.68 \\ 23.43 & -10.50 & -14.15 & -8.09 & -9.27 & 28.57 \\ -16.32 & -23.12 & 95.61 & -47.27 & -4.37 & 5.48 \\ 0.55 & 17.01 & -27.90 & 10.37 & 34.22 & -24.26 \\ -25.75 & 21.80 & -15.49 & 63.26 & -0.19 & -33.63 \end{bmatrix} \quad (46)$$

## V. Results in Time Domain

This section presents time-domain simulations to show the efficacy of the controllers presented in the preceding section to mitigate inter-area oscillations in the test system. To determine the effect that the controllers have on the stability of the system four cases are considered:

- No control case, corresponds to the open loop case where the gain $K$ can be interpreted as a matrix with all its components set to zero. It is the base case.
- The case where the gain is $K_1$ in (44) obtained from the regular optimal output feedback control.
- The case where the gain is $K_2$ in (45) where the rows add up to zero.
- The case where the gain is $K_3$ in (46) where the rows add up to ten.

Two different disturbance events were employed to evaluate the controller performance. The first event is the tripping at $t = 2$ seconds of the Palo Verde generating unit, Gen. 26, at Bus 61. The second event is the loss of the line connecting Buses 86 and 87 that occurs 2 seconds after the simulation starts. The time simulations presented in this work were generated using the MATLAB-based Power System Toolbox (PST) [40]. In these simulations the load buses were modeled using a ZIP model as proposed by the miniWECC test system where the loads have a 50% active power component.

Figs. 7, 8 show the results for the loss of generation event. Fig. 7a shows the relative speed between Gens. 10 and 21 and Fig. 7b shows the relative speed between Gens. 34 and 14. These signals were selected because they yield, respectively, high observability of the North-South A and Alberta modes. These figures show that the system with no control has a distinct oscillation and that all of the controllers provide effective damping to the oscillation. Fig. 7c shows the machine speed at Gen. 10. Because this is a loss of generation event it can be seen in the base case that the frequency drops and the inter-area oscillation is reflected as variations on top of the large drop in frequency. For the case of the $K_1$ gain, the controller is effective not only in damping the inter-area oscillation but also in mitigating the drop in frequency. For the case where the gain is $K_2$ the inter-area oscillation is damped but the larger drop remains; this is the result of forcing the rows of the optimal gain to add up to zero. For the case of the $K_3$ gain, the controller damps the inter-area oscillation and reduces the frequency deviation of the settling frequency; this is the result of making the rows of the optimal gain add up to 10 which is equivalent to adding droop to the load actuators. Figs. 8b and 8a respectively show the command signal and the load consumption of the load at Bus 11. These results show that the command action to the load when the gain is $K_1$ is at a negative level in steady-state while it is zero for the case where the optimal gain is $K_2$. Note that for loads as an actuator for damping inter-area oscillations the option of $K_2$ is clearly preferable to the option of $K_1$ as the load returns to the value of it as if it were not controlled which entails no effect to the user after the oscillation is damped. If the load achieves its modulation via action of energy storage components, the case where the modulation in steady state is zero is also preferable to other

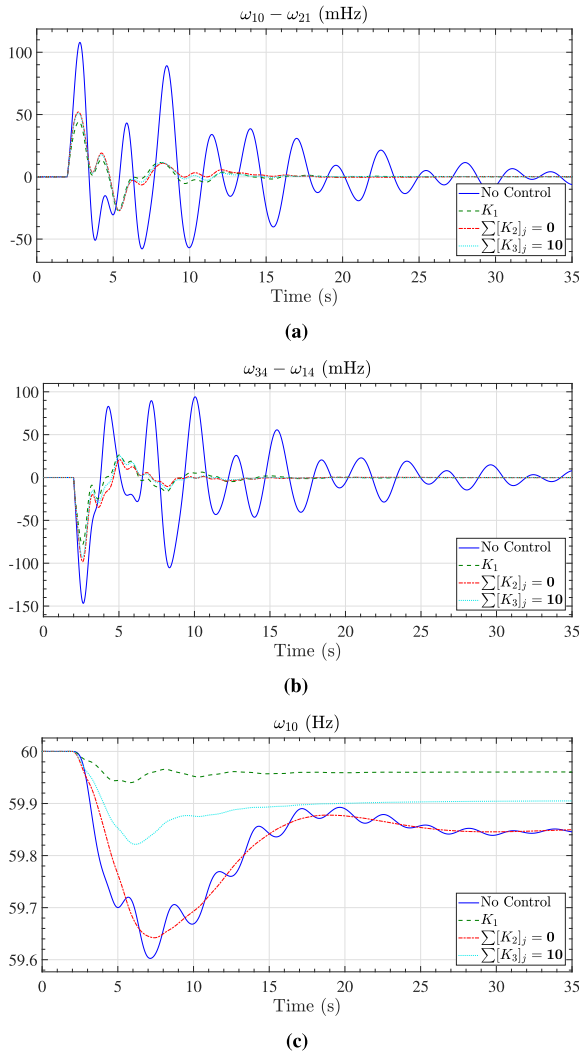


Fig. 7. Generator speed and relative speeds for the loss of generation event at Bus 26. (a) Relative generator speed between Gens. 10 and 21. (b) Relative generator speed between Gens. 34 and 14. (c) Machine speed of generator at Bus 10.

cases because this means that after the event has occurred the energy storage components have neutral power transfer with the grid. The ideal constraint on the gain $K$ is application dependent. If other grid assets provide frequency support, constraining the sum of the gains to zero reduces the steady state support provided by load after a large generator drop. On the other hand, if load must provide frequency support, constraining the sum of the gains to a droop value provides the most benefit to the grid.

Figs. 9, 10 show the results for the loss of line event. Fig. 9a shows the relative speed between Gens. 10 and 21 and Fig. 9b shows the relative speed between Gens. 34 and 14. These results again demonstrate that the system with no control has a poorly damped inter-area oscillation and that the proposed controllers for load clusters effectively mitigate it. Fig. 9c shows the machine speed at Gen. 10.

Figs. 10b and 10a show the command signal and the load consumption of the load at Bus 50 respectively. These figures show the movement the load has to experience to be able to

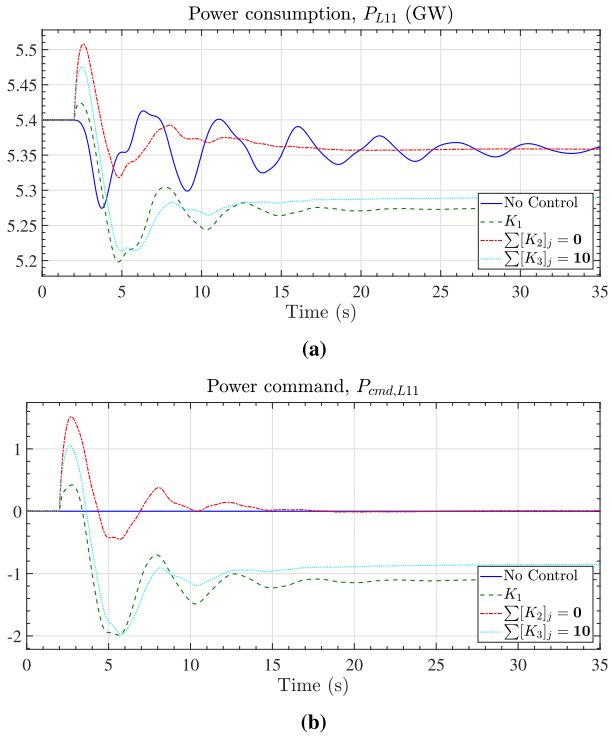


Fig. 8. Load consumption and power command to the load at Bus 11 for the loss of generation event at Bus 26. (a) Load at Bus 11. (b) Power command for the load at Bus 11.

damp the oscillation. For this type of event there is no clear difference in the steady-state command to the loads for the different controllers. The main reason for this result is due to the fact that the settling frequency of the system after the disturbance is very close to the nominal because the disturbance does not cause any significant real power imbalance, the only difference comes from the losses which are marginally modified.

## VI. Effect of System Operating Point

This section presents the effects of the power system operating condition on the performance of the proposed controllers. To this end, the following four different operating conditions were considered:

- **OP1** is the base case and corresponds to the operating condition used for the results in Section V. The power transfer in the California-Oregon Intertie (COI) is set to about 2654 MW.
- **OP2** is the operating condition where the Canadian province of Alberta is disconnected from the system by removing the connection between Buses 6 and 106 in the MiniWECC. This topology change does not significantly affect the COI power transfer which is 2655 MW.
- **OP3** is the case where the power transfer in the COI was increased to 3445 MW. Note that Alberta remained connected in this case.
- **OP4** is the operating condition where the COI power transfer was increased to 3445 MW as in OP3 and Alberta was disconnected from the system as in case OP2.

Note that OP1 was the operating condition considered for designing the controllers in Section IV and testing them in Section V. In this section these controllers are tested under the three new operating conditions OP2, OP3, and OP4.

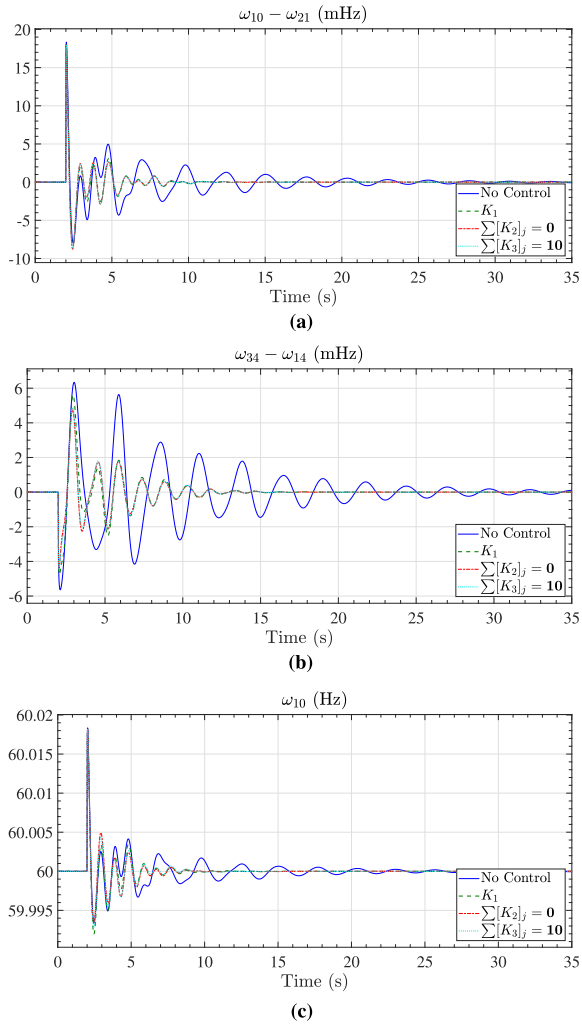


Fig. 9. Generator speed and relative speeds for the loss of line connecting Buses 86 and 87. (a) Relative generator speed between Gens. 10 and 21. (b) Relative generator speed between Gens. 34 and 14. (c) Machine speed of generator at Bus 10.

The behavior of the system under the four different operating conditions without any controller and when the event considered is the loss of Gen. 26 is shown in Fig. 11a. This figure illustrates how the machine speed of Gen. 10 ($\omega_{10}$) is affected by the disturbance under the different operating conditions. This figure shows that the frequency drop caused by the power imbalance similar for all the operating conditions. Note however that OP2, and OP4 (the cases where Alberta is disconnected) exhibit a slightly larger nadir and rate of change of frequency (RoCoF). The results also show that in OP3 and OP4 the inter-area oscillation has less damping; this is expected as these are the cases where the system is more strained because of the increase in the COI power transfer. The case where the inter-area oscillation has almost no damping is OP4 where the COI flow is high and Alberta is disconnected.

Fig. 11b shows $\omega_{10}$ when the second controller ($\sum[K_2]_j = \mathbf{0}$) was included for all the operating conditions. These results show that the controller is able to provide effective damping to the

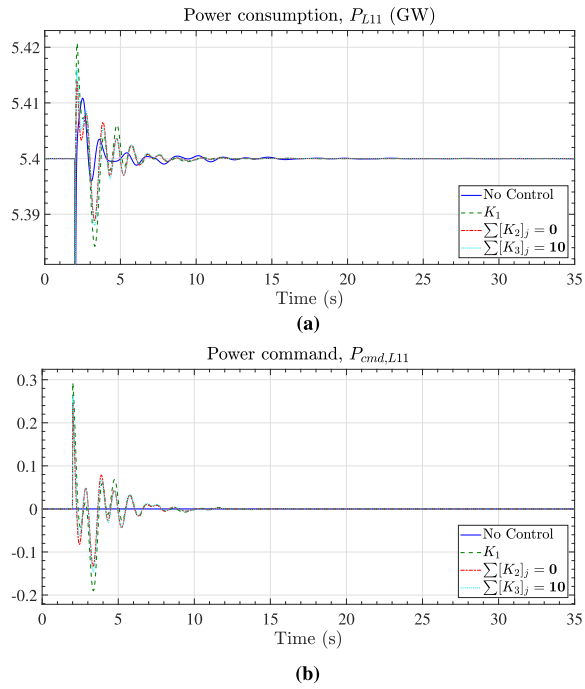


Fig. 10. Load consumption and power command to the load at Bus 50 for the loss of line connecting Buses 86 and 87. (a) Load at Bus 11. (b) Power command for the load a Bus 11.

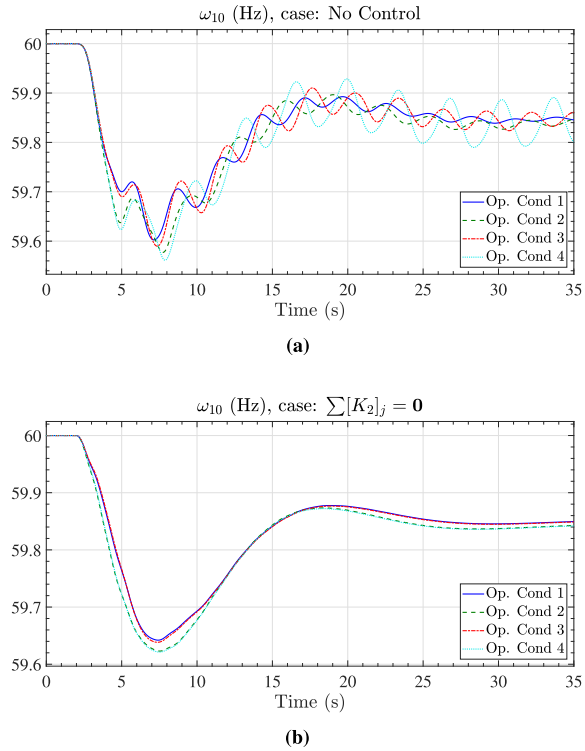


Fig. 11. Machine speed of Gen. 10 for different operating conditions, with and without a controller. (a) Machine speed of Gen. 10 for different operating conditions for the case without a controller. (b) Machine speed of Gen. 10 for different operating conditions for the case where $\sum [K_2]_j = 0$.

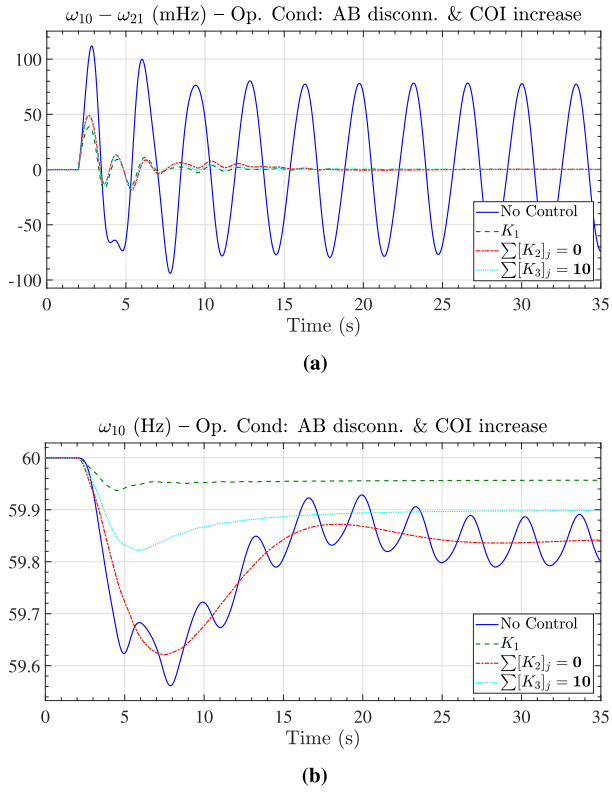


Fig. 12. Generator speed and relative speeds for the operating condition 4. (a) Relative generator speeds between Gens. 10 and 21 for operating condition 4. (b) Machine speed of Gen. 10 for operating condition 4.

system for all the operating conditions even though its design was performed under OP1. Note that with this controller the higher frequency nadir and RoCoF exhibited in OP2 and OP4 is more notorious. This is expected because the inertia and control action of the generating unit in Alberta are no longer present in the system.

Fig. 12 shows the controllers' performances for the loss of Gen. 26 event. Fig. 12a shows the relative speed between Gen. 10 and Gen. 21 for the three controllers designed in Section IV in addition to the no control case for OP4. The results in Fig. 12a show that all the designed controllers provide effective damping to the system and that their performances are similar in terms of relative frequencies. These results align completely with those in Fig. 7a. Fig. 12b shows the machine speed of Gen. 10 individually for the three controllers as well as the no control case. These results show that inter-area oscillations are damped but the settling frequency and frequency nadir differ depending on the controller. These results are in line with those in Fig. 7c and show that the second controller has no influence on the settling frequency because its rows are forced to sum to zero.

## VII. Effect of Load Clustering and Generator Aggregation

This section presents the effect of load clustering and generator aggregation on the effectiveness of the controller. The clusters of loads are determined according to their geographic

TABLE III
LOAD CLUSTERS IN THE MINIWECC BY GEOGRAPHIC LOCATION

| Cluster No. | Region | Loads in the cluster |
|---|---|---|
| 1 | California | $L_{50}$, $L_{55}$, $L_{112}$, $L_{43}$ |
| 2 | PNW | $L_{26}$, $L_{21}$, $L_{36}$, $L_{16}$, $L_{11}$, $L_{29}$ |
| 3 | Canada | $L_8$, $L_{120}$ |
| 4 | Rest | $L_{64}$, $L_{56}$, $L_{95}$, $L_{73}$, $L_{70}$, $L_{109}$, $L_{78}$ |

TABLE IV
GENERATORS AREAS GROUPED BY GEOGRAPHIC LOCATION

| Area No. | Name | Generators in Area |
|---|---|---|
| 1 | California | $G_{21}$, $G_{22}$, $G_{23}$, $G_{19}$, $G_{20}$, $G_{18}$, $G_{17}$, $G_{16}$ |
| 2 | PNW | $G_7$, $G_{14}$, $G_{12}$, $G_9$, $G_8$, $G_5$, $G_6$, $G_{10}$, $G_{11}$, $G_{15}$ |
| 3 | Canada | $G_1$, $G_2$, $G_3$, $G_{34}$ |
| 4 | Rest | $G_{13}$, $G_{14}$, $G_{32}$, $G_{31}$, $G_{33}$, $G_{29}$, $G_{30}$, $G_{24}$, $G_{25}$, $G_{28}$, $G_{27}$ |

location as opposed to the correlation of measurements used in Section IV. Similarly, generators are aggregated into areas defined geographically. The cluster of loads and areas for generator aggregation are the same: California, Pacific Northwest (PNW), Canada, and the rest of the system.[1] Clustering the loads and aggregating the generators geographically was decided because this grouping is the most intuitive and it is potentially the easiest to accomplish due to the different regulating bodies in different parts of the US Western Interconnection. The geographic clustering of loads and generator aggregation is presented in Tables III and IV, respectively.

Using the load clusters in Table III and the generator areas in Table IV a new system was identified using the approach described in Section II. Equivalent stabilizing controllers as those in Section IV were designed and the controller gains are presented in equations (47) to (49). Note that because the number of load clusters is the same as the generator areas the new controller gains are square matrices. Note also that the operating condition used in this Section is OP1.

$$K_{1,\text{geo}} = \begin{bmatrix} 54.69 & 0.77 & -13.33 & 2.63 \\ -4.32 & 51.21 & -4.31 & -7.09 \\ -3.03 & -30.87 & 47.16 & 3.71 \\ 6.38 & -34.45 & -13.19 & 71.95 \end{bmatrix} \quad (47)$$

$$K_{2,\text{geo}} = \begin{bmatrix} 41.10 & -3.23 & -21.72 & -16.15 \\ -14.55 & 47.10 & -10.58 & -21.97 \\ -8.11 & -32.29 & 43.74 & -3.34 \\ -2.91 & -37.02 & -19.08 & 59.02 \end{bmatrix} \quad (48)$$

$$K_{3,\text{geo}} = \begin{bmatrix} 44.15 & -2.35 & -19.91 & -11.90 \\ -11.69 & 48.31 & -8.86 & -17.75 \\ -5.13 & -31.35 & 45.58 & 0.90 \\ 0.09 & -36.16 & -17.26 & 63.33 \end{bmatrix} \quad (49)$$

Fig. 13 presents each controllers' performance designed using different clustering methods. The event analyzed is the loss of Gen. 26 in the Southwest. Fig. 13a presents the machine speed of Gen. 10 with the controllers $K_1$ and $K_{1,\text{geo}}$. Fig. 13b presents the machine speed of Gen. 10 for the case where the controllers, $K_2$ and $K_{2,\text{geo}}$, have the sum of their rows equal to zero. Fig. 13c presents the machine speed of Gen. 10 for the case where rows of the controllers add up to 10, these controllers are noted $K_3$ and $K_{3,\text{geo}}$. The results in Fig. 13 show that the controllers designed using the geographic clustering provide a similar damping effect to those designed in Section IV. Fig. 14a shows the relative machine speed between Gens. 10 and 21 when the three stabilizing controllers, designed using the geographic clustering and aggregation, are included in the system. This figure shows that the system inter-area oscillations are well damped by any of the proposed controllers. The results for the same type of

[1]That is, all the loads and generators that do not belong to any of the other three areas were grouped into an area.

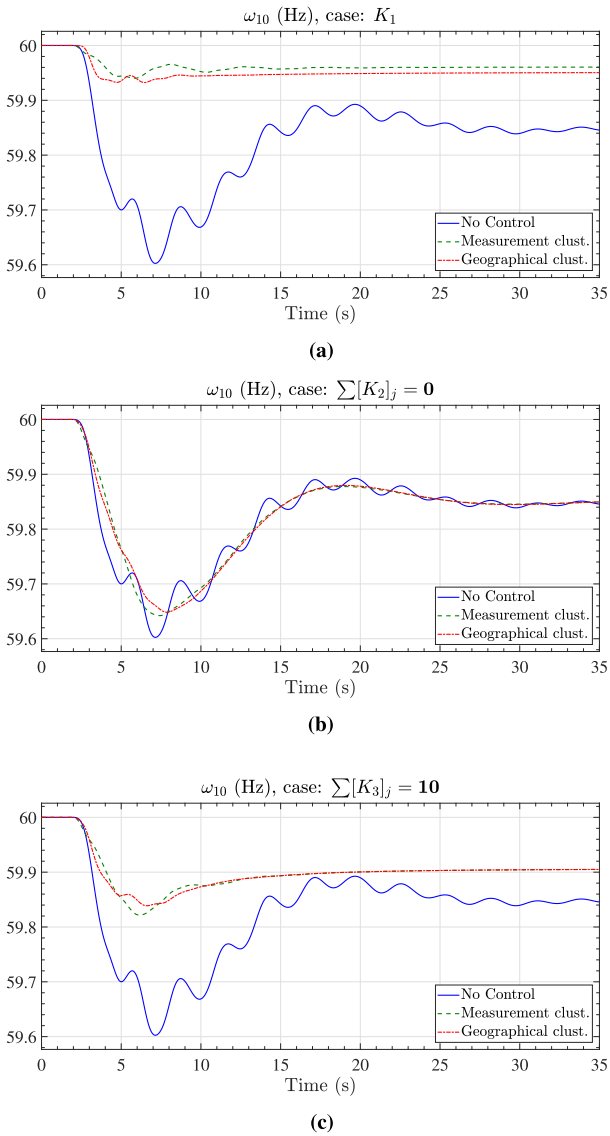


Fig. 13. Machine speed of generator at Bus 10 for the loss of generation event at Bus 26. Comparison of the different cases of clustering. (a) Machine speed of generator at Bus 10 for the case of $K_1$. (b) Machine speed of generator at Bus 10 for the case of $\sum [K_2]_j = 0$. (c) Machine speed of generator at Bus 10 for the case where $\sum [K_3]_j = 10$.

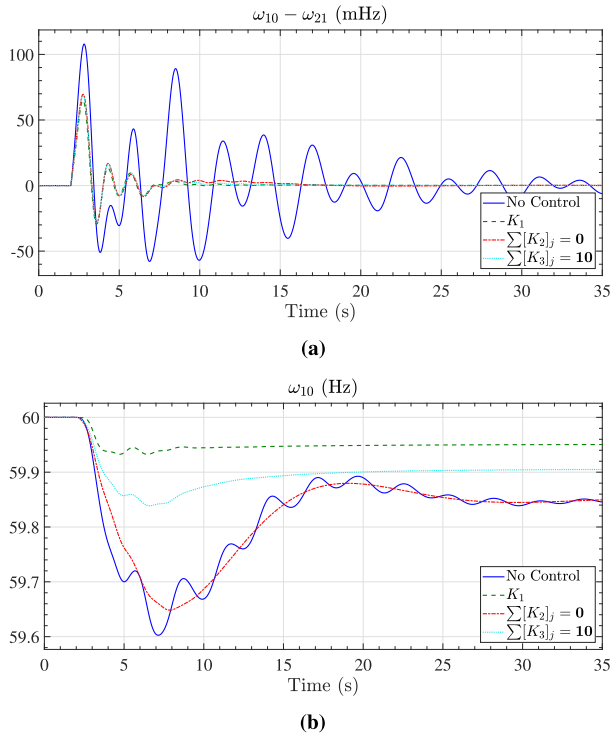


Fig. 14. Generator speed and relative speeds for the loss of Gen. 26. Geographical clustering was used for both load and generation. (a) Relative generator speed between Gens. 10 and 21. (b) Machine speed of generator at Bus 10.

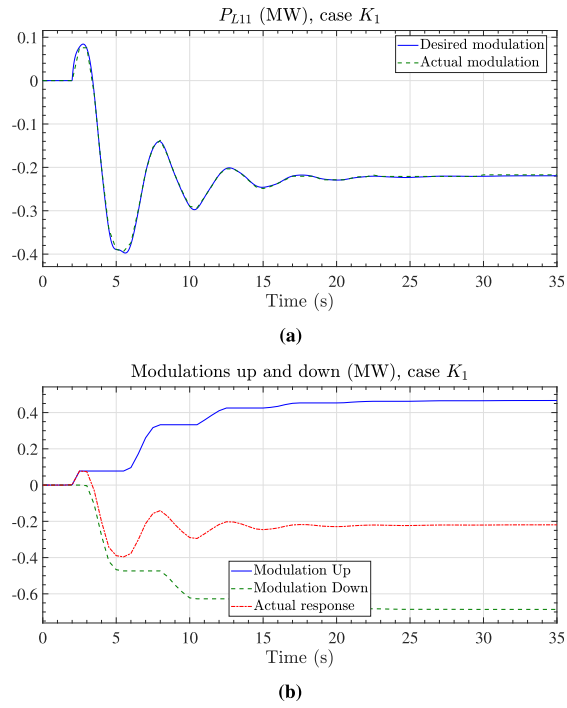


Fig. 15. Desired and actual load modulation with a detailed load model based on a population of 1000 residential air conditioners. (a) Load at Bus 11 when the controller gain is $K_1$. (b) Modulation up and down at $L_{11}$ when the controller gain is $K_1$.

disturbance using the controllers presented in Section IV are shown in Fig. 7a. Comparing the results in these two figures shows that the initial first swing is smaller for the case of the controllers in Section IV. The relative frequency reaches 50 mHz while it goes to almost 70 mHz for the case of the controllers presented in this section. The damping provided is similar with the oscillation almost vanishing at around 10 seconds for both cases of stabilizing controllers. Fig. 14b shows the machine speed of Gen. 10 when the stabilizing controllers proposed in this section are included in the system. These results are comparable to those in Fig. 7c. The results in Fig. 14b show that the primary frequency response of the system is different depending on the control case. In particular, the settling frequency is affected by the control selected and just as in Fig. 7c the second controller does not act in steady-state. The first and third controller provide an action that is helpful to the system in steady state with the action of the third controller being determined by the constrained optimization ($\sum[K_3]_j = \mathbf{10}$).

## VIII. Modulation of Detailed End-Use Load Models

This section shows how aggregator-level load modulation can be realized with detailed end-use load models. The device level control strategy for following the aggregator-level modulation is detailed in [24] and is organized in two separate layers. A device layer where individual load devices activate or deactivate themselves depending on whether a control signal, determined by the supervisory layer, exceeds a predetermined local threshold. A supervisory layer that selects these local thresholds to ensure the aggregated load response follows the power modulation signal.

Figs. 15 and 16 show the results of applying the device-level control strategy in [24] to deliver the aggregator-level power modulation signals in Fig. 8. In the simulation, 1000 residential air conditioners (AC) were considered for the purpose of illustration. Because the modulation in Fig. 8 a is in the order of the hundreds of MW (around 0.4 GW maximum in the $K_2$ case), the signal was scaled down so a population of 1000 ACs can follow the signal. Fig. 15 a shows the desired modulation signal and the actual modulation delivered with the end-use load control for the commanded signal for the load at Bus 11 for the $K_1$ control gain case. Fig. 16 a presents the same results as Fig. 15 a but for the $K_2$ control gain case. The results show that the aggregated load response can properly follow the modulation signal throughout the simulation for both cases considered. Fig. 15 b shows the effective modulation up and down of the population of AC to deliver the desired load response when the controller is defined by gain $K_1$. Fig. 16 b shows the effective modulation up and down of the population of AC to deliver the desired load response when the controller is defined by gain $K_2$. Note that Fig. 15 b shows that more power is provided by the modulation down in steady state. This means that in this case, when the gain is $K_1$, the population of ACs end up less room to provide modulation down should another event occur. In contrast, the results in Fig. 16 b show that the final modulation up has the same magnitude as the final modulation down and is the result of making the rows of the optimal gain, $K_2$, add up to zero. This means the population

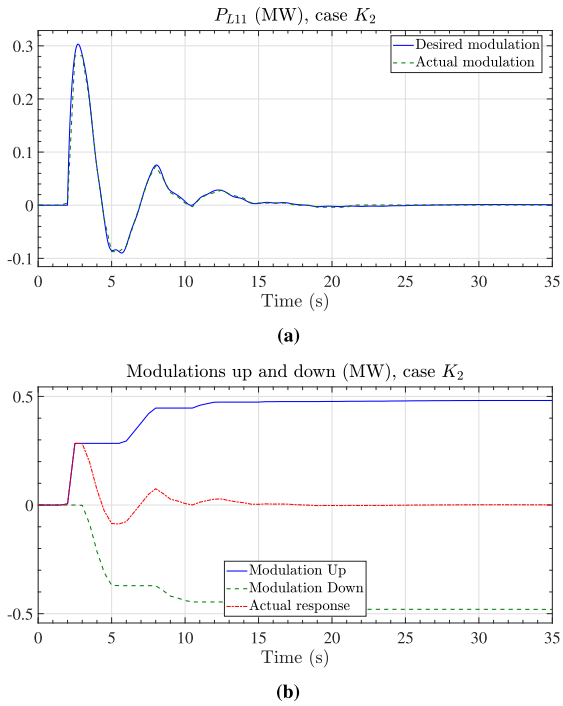


Fig. 16. Desired and actual load modulation with a detailed load model based on a population of 1000 residential air conditioners. (a) Load at Bus 11 when the controller gain is $K_2$. (b) Modulation up and down at $L_{11}$ when the controller gain is $K_2$.

of AC units can provide the same amount of modulation after the event.

## IX. Conclusion and Future Work

This paper develops a methodology to use loads, or the demand side of the system, to damp inter-area oscillations in power systems. In this methodology, clusters of loads are used to initially determine a state-space representation of the system. Using this representation a regular optimal output feedback control (OOFC) is calculated. The paper proposes an extension to the OOFC approach to ensure that the rows of the optimal gain add up to a scalar value. Three different control designs were presented: conventional OOFC damping control (frequency droop gain not specified); OOFC damping control with no frequency droop (sum of gain rows equals 0); and OOFC damping control with a specified frequency droop gain. Time domain simulations in a large-scale power system are used to illustrate the effectiveness of these controllers. These simulations show that clusters of loads are able to provide effective damping to the system inter-area oscillations. Time simulations for different operating points of the system show that the proposed control strategies are still effective in stabilizing the system. In addition, it is shown that different ways of clustering loads can provide similar damping to inter-area oscillations. The results also confirm that in the case of OOFC damping control with the frequency droop gain constrained to zero the loads only act during the initial disturbance after a loss of generation, which is the expected behavior. The paper also shows that the modulation signal can be delivered using detailed end-use load models.

Future lines of research include: determining the effects of communication delays have on the proposed controller; investigating the optimal clustering loads and generators; and dispatch prioritization of loads within a cluster.

## Acknowledgment

Sandia National Laboratories is a multimission laboratory managed and operated by National Technology and Engineering Solutions of Sandia, LLC., a wholly owned subsidiary of Honeywell International, Inc., for the U.S. Department of Energy's National Nuclear Security Administration under contract DE-NA0003525.

Pacific Northwest National Laboratory is operated by Battelle for the U.S. Department of Energy under Contract DE-AC05-76RL01830.

The views expressed in the article do not necessarily represent the views of the U.S. Department of Energy or the United States Government.

## References

[1] G. Rogers, *Power System Oscillations*. Boston, MA, USA: Springer, 2012.
[2] D. N. Kosterev, C. W. Taylor, and W. Mittelstadt, "Model validation for the August 10, 1996 WSCC system outage," *IEEE Trans. Power Syst.*, vol. 14, no. 3, pp. 967–979, Aug. 1999.
[3] D. Trudnowski, D. Kosterev, and J. Undrill, "PDCI damping control analysis for the Western North American power system," in *Proc. IEEE Power Energy Soc. Gen. Meet.*, Vancouver, BC, Canada, 2013, pp. 1–5.
[4] *IEEE Tutorial Course - Power System Stabilization via Excitation Control*, IEEE Power & Energy Soc., Piscataway, NJ, USA, 2007.
[5] J. H. Chow, J. J. Sanchez-Gasca, H. Ren, and S. Wang, "Power system damping controller design using multiple input signals," *IEEE Control Syst. Mag.*, vol. 20, no. 4, pp. 82–90, Aug. 2000.
[6] Y. Zhang and A. Bose, "Design of wide-area damping controllers for inter-area oscillations," *IEEE Trans. Power Syst.*, vol. 23, no. 3, pp. 1136–1143, Aug. 2008.
[7] B. Chaudhuri, R. Majumder, and B. C. Pal, "Wide-area measurement-based stabilizing control of power system considering signal transmission delay," *IEEE Trans. Power Syst.*, vol. 19, no. 4, pp. 1971–1979, Nov. 2004.
[8] F. Dörfler, M. R. Jovanović, M. Chertkov, and F. Bullo, "Sparsity-promoting optimal wide-area control of power networks," *IEEE Trans. Power Syst.*, vol. 29, no. 5, pp. 2281–2291, Sep. 2014.
[9] M. E. Raoufat, K. Tomsovic, and S. M. Djouadi, "Dynamic control allocation for damping of inter-area oscillations," *IEEE Trans. Power Syst.*, vol. 32, no. 6, pp. 4894–4903, Nov. 2017.
[10] A. Chakrabortty, "Wide-area damping control of power systems using dynamic clustering and TCSC-based redesigns," *IEEE Trans. Smart Grid*, vol. 3, no. 3, pp. 1503–1514, Sep. 2012.
[11] N. Yang, Q. Liu, and J. D. McCalley, "TCSC controller design for damping interarea oscillations," *IEEE Trans. Power Syst.*, vol. 13, no. 4, pp. 1304–1310, Aug. 1998.
[12] N. Mithulananthan, C. A. Canizares, J. Reeve, and G. J. Rogers, "Comparison of PSS, SVC, and STATCOM controllers for damping power system oscillations," *IEEE Trans. Power Syst.*, vol. 18, no. 2, pp. 786–792, May 2003.
[13] J. Fang, W. Yao, Z. Chen, J. Wen, and S. Cheng, "Design of anti-windup compensator for energy storage-based damping controller to enhance power system stability," *IEEE Trans. Power Syst.*, vol. 29, no. 3, pp. 1175–1185, May 2014.
[14] J. C. Neely *et al.*, "Damping of inter-area oscillations using energy storage," in *Proc. IEEE Power Energy Soc. Gen. Meeting*, Vancouver, BC, Canada, 2013, pp. 1–5.
[15] M. Singh, A. J. Allen, E. Muljadi, V. Gevorgian, Y. Zhang, and S. Santoso, "Interarea oscillation damping controls for wind power plants," *IEEE Trans. Sustain. Energy*, vol. 6, no. 3, pp. 967–975, Jul. 2014.
[16] K. Liao, Z. He, Y. Xu, G. Chen, Z. Y. Dong, and K. P. Wong, "A sliding mode based damping control of DFIG for interarea power oscillations," *IEEE Trans. Sustain. Energy*, vol. 8, no. 1, pp. 258–267, Jan. 2016.

[17] F. Wilches-Bernal, C. Lackner, J. H. Chow, and J. J. Sanchez-Gasca, "Effects of wind turbine generators on inter-area oscillations and damping control design," in *Proc. 52nd Hawaii Int. Conf. Syst. Sci.*, 2019, pp. 3649–3658.
[18] H. Li *et al.*, "Damping control strategies of inter-area low-frequency oscillation for DFIG-based wind farms integrated into a power system," *Int. J. Elect. Power Energy Syst.*, vol. 61, pp. 279–287, Oct. 2014.
[19] L. Zhou *et al.*, "Damping inter-area oscillations with large-scale PV plant by modified multiple-model adaptive control strategy," *IEEE Trans. Sustain. Energy*, vol. 8, no. 4, pp. 1629–1636, Oct. 2017.
[20] R. Byrne *et al.*, "Small signal stability of the Western North American power grid with high penetrations of renewable generation," in *Proc. IEEE 43rd Photovolt. Specialists Conf.*, 2016, pp. 1784–1789.
[21] B. J. Pierre *et al.*, "Design of the pacific dc intertie wide area damping controller," *IEEE Trans. Power Syst.*, vol. 34, no. 5, pp. 3594–3604, Sep. 2019.
[22] M. A. Elizondo *et al.*, "Interarea oscillation damping control using high-voltage dc transmission: A survey," *IEEE Trans. Power Syst.*, vol. 33, no. 6, pp. 6915–6923, Nov. 2018.
[23] D. Trudnowski *et al.*, "Initial closed-loop testing results for the pacific DC intertie wide area damping controller," in *Proc. IEEE Power Energy Soc. Gen. Meeting*, Chicago, IL, USA, 2017, pp. 1–5.
[24] J. Lian *et al.*, "Universal wide-area damping control for mitigating inter-area oscillations in power systems," Pacific Northwest National Laboratory, Richland, WA, USA, Tech. Rep. PNNL-27351, 2017.
[25] J. Lian, Q. Zhang, L. D. Marinovici, R. Fan, and J. Hansen, "Wide-area demand-side control for inter-area oscillation mitigation in power systems," in *Proc. IEEE Transmiss., Distrib., Conf. Expo.*, Denver, CO, USA, 2018, pp. 1–5.
[26] C. Zhang, D. Ke, Y. Sun, C. Chung, and J. Xu, "Investigations of large-scale voltage-dependent loads for damping inter-area oscillations: Mechanism and robust decentralized control," *IEEE Trans. Power Syst.*, vol. 33, no. 6, pp. 6037–6048, Nov. 2018.
[27] J.-N. Juang and R. S. Pappa, "An Eigensystem realization algorithm for modal parameter identification and model reduction," *J. Guid., Control, Dyn.*, vol. 8, no. 5, pp. 620–627, 1985.
[28] WECC Joint Synchronized Information Subcommittee, "Modes of inter-area power oscillations in western interconnection," Western Electricity Coordinating Council, Salt Lake City, UT, USA, Tech. Rep., 2013, [Online]. Available: https://www.wecc.org/Reliability/WECC%20JSIS%20Modes%20of%20Inter-Area%20Oscillations-2013-12-REV1.1.pdf
[29] R. Concepcion, F. Wilches-Bernal, and R. H. Byrne, "Effects of communication latency and availability on synthetic inertia," in *Proc. IEEE Innovative Smart Grid Technol. Conf.*, 2017, pp. 1–5.
[30] F. Wilches-Bernal, R. Concepcion, and R. H. Byrne, "Impact of communication latencies and availability on droop-implemented primary frequency regulation," in *Proc. IEEE North Amer. Power Symp.*, Morgantown, WV, USA, 2017, pp. 1–5.
[31] L. Ljung, *System Identification, Theory for the User*. Upper Saddle River, NJ, USA: Prentice-Hall, 1998.
[32] J. J. Sanchez-Gasca and J. H. Chow, "Performance comparison of three identification methods for the analysis of electromechanical oscillations," *IEEE Trans. Power Syst.*, vol. 14, no. 3, pp. 995–1002, Aug. 1999.
[33] B. D. Anderson and J. B. Moore, *Linear Optimal Control*, vol. 197. Englewood Cliffs, NJ, USA: Prentice-Hall, 1971.
[34] J. Bernussou and J. Geromel, "An easy way to find gradient matrix of composite matricial functions," *IEEE Trans. Autom. Control*, vol. 26, no. 2, pp. 538–540, Apr. 1981.
[35] W. Hutcheson, "A simple derivation of the gradient conditions for optimal constant output feedback gains," *IEEE Trans. Autom. Control*, vol. 23, no. 5, pp. 937–938, Oct. 1978.
[36] J. C. Geromel, "Contribution à l'étude des systèmes dynamiques interconnectés: Aspects de décentralisation," Ph.D. dissertation, Université Paul Sabatier-Toulouse III, Toulouse, France, 1979.
[37] T. Rautert and E. W. Sachs, "Computational design of optimal output feedback controllers," *SIAM J. Optim.*, vol. 7, no. 3, pp. 837–852, 1997.
[38] F. Wilches-Bernal, D. A. Copp, G. Bacelli, and R. H. Byrne, "Structuring the optimal output feedback control gain: A soft constraint approach," in *Proc. IEEE Conf. Decis. Control*, 2018, pp. 2464–2469.
[39] D. Trudnowski and J. Undrill, *Oscillation Damping Controls, Year 1 Report of Bonneville Power Administration Contract 37508*, Sep. 2008, ch. The MinniWECC System Model.
[40] J. H. Chow and K. W. Cheung, "A toolbox for power system dynamics and control engineering education and research," *IEEE Trans. Power Syst.*, vol. 7, no. 4, pp. 1559–1564, Nov. 1992.

**Felipe Wilches-Bernal** (S'12–M'16) received the M.S. degree in control systems and signal processing from Université Paris-Sud XI, Orsay, France, and the Ph.D. degree in electrical engineering from Rensselaer Polytechnic Institute, Troy, NY, USA. In 2015, he joined the Electric Power Systems Research Department, Sandia National Laboratories, Albuquerque, NM, USA, where he currently works as a Senior Member of Technical Staff. Since joining in Sandia, he has been a key technical contributor and PI/Co-PI of multiple projects in the power systems integration area. His research experience and interests include power system stability and control, renewable energy and smart grid technologies, and signal processing and control techniques applied to power systems. He was a key contributor of the team that was awarded the 2017 R&D 100 award for developing a control system for active damping of inter-area oscillations.

**Raymond H. Byrne** (S'86–M'89–SM'07–F'17) received the B.S. degree in electrical engineering from the University of Virginia, Charlottesville, VA, USA, the M.S. degree in electrical engineering from the University of Colorado, Denver, CO, USA, the M.S. degree in financial mathematics (financial engineering) from The University of Chicago, Chicago, IL, USA, and the Ph.D. degree in electrical engineering from The University of New Mexico, Albuquerque, NM, USA. He is currently the Manager of the Electric Power Systems Research Department, Sandia National Laboratories, Albuquerque, NM, USA, where he has been employed since 1989. He also serves as the Team Lead of the Equitable Regulatory Environment thrust area of the Sandia energy storage program. His awards include Time Magazine Invention of the Year in Robotics in 2001 and the Prize Paper Award at the 2016 IEEE Power and Energy Society General Meeting for a paper on "Maximizing revenue from energy storage in grid applications." He is a member of Tau Beta Pi, Eta Kappa Nu, and Sigma Xi. He was elevated to IEEE Fellow for contributions to miniature robotics and grid integration of energy storage in 2017.

**Jianming (Jamie) Lian** (S'09–M'10) received the B.S. degree with the highest honor from the University of Science and Technology of China, Hefei, China, in 2004, and the M.S. and Ph.D. degrees in electrical engineering from Purdue University, West Lafayette, IN, USA, in 2007 and 2009, respectively. From 2010 to 2011, he was a Postdoctoral Research Associate with the Center for Advanced Power Systems, Florida State University, Tallahassee, FL, USA, where he was involved in various projects related to the development of future all-electric ship supported by ONR. He is currently a Senior Staff Engineer leading the Analysis Team of the Optimization and Control Group, Pacific Northwest National Laboratory (PNNL). Since joining in PNNL, he has been a Project Manager, PI/Co-PI and key technical contributor of many research projects in the areas of power grid, building system, and transportation network. His research focuses on the application of interdisciplinary principles from control, optimization, microeconomics, game, and learning to improve the reliability and resiliency of large-scale complex systems.